A Sliding Mode Missile Pitch Autopilot Synthesis for High Angle of Attack Maneuvering

Ajay Thukral and Mario Innocenti, *Member, IEEE*

***Abstract*— A new approach to the synthesis of longitudinal autopilots for missiles flying at high angle of attack regimes is presented. The methodology is based on sliding mode control, and uses a combination of aerodynamic surfaces and reaction jet thrusters, to achieve controllability beyond stall. The autopilot is tested on a small section of the flight envelope consisting of a fast 180° heading reversal in the vertical plane, which requires robustness with respect to uncertainties in the system's dynamics induced by large variations in dynamic pressure and aerodynamic coefficients. Nonlinear simulation results show excellent performance and capabilities of the control system structure.**

***Index Terms*— Control systems, missile control, robustness, scheduling, variable structure systems.**

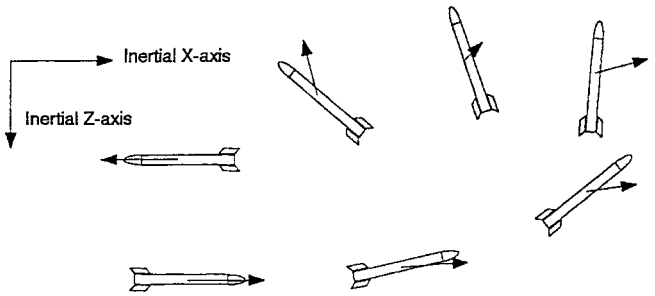

Fig. 1. Heading reversal maneuver.

I. Introduction

THE feasibility of combining traditional aerodynamic control with reaction jets in the framework of missile autopilot design is addressed in this paper. The purpose of propulsive actuation is mainly to increase the angle of attack envelope for improved turn rate capabilities and maneuverability. Due to nonlinear characteristics of both controller and airframe dynamics, aerodynamic and geometric model uncertainties, a control strategy based on variable structure systems is used. A control law is then synthesized for a pitch channel autopilot and used in a post stall maneuver after launch.

Future missile systems will be required to possess higher turn rates and larger maneuverability envelopes, while simultaneously requiring reduced storage and signature volumes. In this respect, efforts are under way to evaluate alternate means of missile control as opposed to purely aerodynamic control [1], [2]. Several technology payoffs can be envisioned if alternate control strategies are implemented, among which there are:

- smaller fin sizes that decrease stowage volume for internal carriage, especially important for the type of fighters currently being developed;
- increased maneuverability and off-boresight capability for an improved all-aspect defensive shield;
- high angle of attack launch capability to match improved aircraft agility;
- improved end-game performance (higher g-levels).

Manuscript received August 2, 1995; revised January 12, 1998. Recommended by Associate Editor, F. Y. Hadaegh. This work was supported in part by Research Development Laboratories Grant RDL-93-132.

A. Thukral is with the Mechanical Engineering Department, Tuskegee University, AL 36088 USA.

M. Innocenti is with the Department of Electrical Systems and Automation (DSEA), University of Pisa, 56126 Pisa, Italy.

Publisher Item Identifier S 1063-6536(98)03003-6.

The achievement of these payoffs poses difficult challenges to the control system designer that encompass all phases of flight. For example, during separation from the launch aircraft, an increase in pitch-up tendencies can be expected due to lack of sufficient aerodynamic stabilization (smaller fins). After safe separation, the system may be required to perform fast 180° turns to defend against and engage rear-hemisphere positioned threats and targets. During the end-game, the reduced aerodynamic control effectiveness due to smaller fin sizes must be appropriately compensated in order to generate sufficient load factors in a very short time.

The desire to limit cross section and volume (smaller diameters and smaller fin sizes) drastically reduces the amount of aerodynamic effectiveness of the missile. This loss in control power must be compensated for and/or improved by using alternate control technologies. Possible options are propulsion-based control in the form of thrust vectoring (TVC) and/or a reaction jet control system (RCS). The potential modifications involving the implementation of propulsion control and its integration with aerodynamic surfaces are several, and their description and implications are beyond the scope of the present paper. Just to summarize some of the aspects, however, we mention the technology involved with the design of each component, as well as the integration of elements leading to variable degree of effort: from the mere addition of an actuator on an existing airframe, all the way to a new missile design. The work presented herein concentrates on only one of the propulsive solutions, the use of reaction jets. The application of thrust vector control is addressed elsewhere [3].

This paper is structured as follows: Section II presents the test scenario used for the evaluation of the autopilot. The dynamic models of the vehicle and the autopilot synthesis are described in Sections III and IV, respectively. Section V describes the system's performance based on a nonlinear

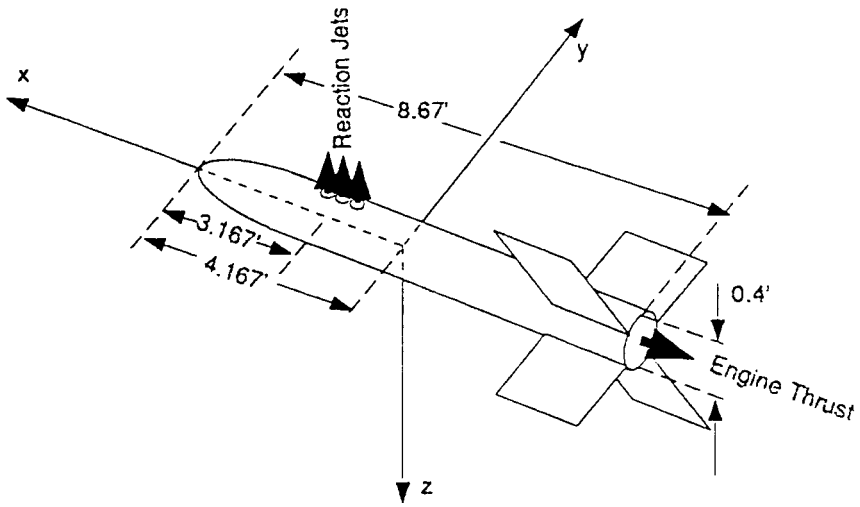

Fig. 2. Missile configuration.

computer simulation. Finally, the conclusions are summarized in Section VI.

II. Maneuver Description

In order to gain appreciation for some of the problems involving reaction jet control and its blending with traditional aerodynamic control, a high angle of attack (high alpha) maneuver was chosen as test scenario. In particular, a two-dimensional heading reversal trajectory in the longitudinal plane was selected as typical of a defensive maneuver against tail and fly-by threats, as shown schematically in Fig. 1. The trajectory can be thought as representative of initial phase enhanced maneuvering capability, or to be used during midcourse flight path changes provided the missile has multiinjection engine capabilities. Many challenges to guidance and control systems are posed by the above selection and some of the critical issues are addressed here leading to a preliminary design of the autopilot.

The maneuver is a 180° off-boresight trajectory with turn rates of the order of 80°/s. The missile flies as quickly as possible along a minimum radius turn path, and in a time frame of the order of 2 s. Flying this maneuver impacts both the guidance and autopilot subsystems. The guidance aspects deal with the generation of an appropriate flight path command along which the missile turns changing its heading and attitude of up to and exceeding 180°. The selection of this path could depend on agility and/or tactical issues. The autopilot aspects deal with the control of forces and moments on the missile, capable of generating accelerations and attitude rates required by the guidance system. Appropriate blending of aerodynamic and reaction jet controls may be required since, during parts of the trajectory, the missile may experience loss of lifting capabilities due to angles of attack much higher than stall.

In this paper we do not address the question of guidance law design, rather we present the development of a nonlinear autopilot logic capable of implementing the maneuver, and a blending strategy which uses aerodynamic control at low angles of attack and RCS control when the missile's angle of attack is beyond stall. Since the main purpose of the work is to show the feasibility of the autopilot logic under high alpha conditions, the control law is synthesized based on modeling assumptions that may not hold for an extended flight envelope, namely accurate nonlinear aerodynamics and flexibility effects. Further refinement of the control system will require the inclusion of those effects, which are beyond the scope of the paper at this point.

III. Model Derivation

The selected test maneuver requires two widely different dynamic behaviors caused by stalled and unstalled flows about the vehicle. The stalled state is representative of a small lift with a very large form drag accompanied by loss of conventional aerodynamic control surfaces. The missile model during this part of the maneuver is described by pure pitching motion and point mass dynamics. In the unstalled condition the aerodynamic interaction is predominant generating large lift forces with small drag. The standard short period dynamics are used, provided some reasonable assumptions are made on their usage and validity.

The system dynamic models are based on a generic air-to-air configuration corresponding to a standard cruciform axial-symmetric shape shown in Fig. 2. Preliminary analyzes [1], [2] indicated that structural flexibility was not a crucial issue for such geometry, in spite of expected large load factors during the chosen maneuver since the first bending mode natural frequency was estimated to be of the order of 30 Hz. However, it is expected that other phases of the envelope, terminal homing in particular, may require the presence of notch filters in order to attenuate sensor signals around that frequency. The presence of filtering, of course will lead to an upper limit on the available flight control bandwidth, slowing down the system's response and hindering the autopilot capabilities. Since our attention is concentrated on the "best performance" autopilot within a restricted phase of flight, the missile was modeled as a rigid body, leaving a more accurate analysis, with flexibility

TABLE I
PHYSICAL AND GEOMETRIC CHARACTERISTICS

L_{REF}	0.4167 ft
S	0.1367 ft^2
mass	7.0 slugs
$I_Y = I_Z$	51.0 sl-ft^2
I_X	0.229 sl-ft^2
Fins	X configuration
L_{RCS}	3.167 ft from tip
x_{cg}	4.167 ft from tip
Length	8.67 ft
Diameter	0.4 ft

TABLE II
MISSILE AND FLIGHT CONDITION DATA

Main Engine Nominal Thrust	T_E = 5,000 lbs
Reaction Jets Nominal Thrust	T_{RCS} = 500 lbs
RCS Time Constant	τ_u = 1/500 sec
Elevator Time Constant	τ_δ = 1/180 sec
RCS Deadband	variable by design
Launch Mach Number	M = 0.8
Launch Altitude	h = 10,000 ft
Initial Angle of Attack	10 degrees
Initial Attitude	10 degrees

included, for further work. The main geometric characteristics of the configuration are listed in Table I.

The propulsion system consists of an RCS and a main engine. The location, size, and detailed operational characteristics of the thrusters are not discussed here in any detail, and the interaction between aerodynamic flow and jet plumes has been neglected as well. For the purpose of the present study, the actuation characteristics of the thrusters were modeled as those of a typical relay, with a constant output thrust, chosen nominally as 500 lbs, and a first-order lag with a time constant of about 2 ms.

The main engine, which in principle could have thrust vectoring capabilities, was assumed operating at a nominal thrust $T_E = 5000$ lbs. The engine was used in order to recover the dynamic pressure lost due to the drag increase a high angles of attack, and to provide velocity vector rotation. The burn time interval during this phase could be considered as a design parameter, in addition to the RCS thrust level and location. The nominal launch flight condition was chosen to be that of Mach 0.8 and altitude of 10 000 ft. A summary of flight condition and propulsion data is given in Table II.

The aerodynamic control forces and moments are generated by deflecting fins positioned in a standard X-tail configuration. Since the test maneuver is confined to the longitudinal plane, the computation of applied forces and moments does not include lateral-directional effects. This simplification implies a complete decoupling between the longitudinal and latero-directional axes. Although our attention is confined to the longitudinal autopilot, channel cross-couplings and integration need to be verified in subsequent designs, especially at high angles of attack, where, in addition to inertial cross couplings, vortex separation, and unsteady phenomena will produce crossfeeds, whose contribution may limit channel separation.

A. Aerodynamic Data

The aerodynamic forces and moments are usually obtained from wind tunnel data of the vehicle and then "tuned" using flight testing. *The uncertainty and parameter variations introduced this way were then used to test the robustness test of the variable structure controller.*

In the maneuver chosen as the test scenario for autopilot validation, the vehicle flies through a wide range in angles of attack. Missile DATCOM code [4] was used for low angles of attack (assumed predefined by $\alpha < 40°$). For the stalled condition, analytical methods [5]. Linear interpolation was then performed on the aerodynamic data.

At high angles of attack, the missile behaves as a bluff body causing flow separation, and a large wake behind the body. The predominant component of the drag force is pressure drag. The estimation of the aerodynamic forces was done assuming the missile as a cylinder and neglecting the interference effect between wings and main body, as a first approximation. The main aerodynamic force at high angles of attack is the normal force N, which contributes almost exclusively to the drag. The normal force coefficient $C_N = N/QS$, where Q is the dynamic pressure and S the reference area, is a function of angle of attack, Reynolds number, and Mach number. The coefficient C_N was first computed as a function of Reynolds number, at zero angle of attack and constant Mach number, then modified accordingly. Based on the above assumptions, a code was written to obtain aerodynamic data for high alpha values, details can be found in [6]. Defining with S' the frontal area of the cylinder, and with S the vehicle cross-sectional area, the aerodynamic coefficients can be expressed as functions of the angle of attack α as [5]

$$\begin{cases} C_N = C_N\left(\dfrac{S'}{S}\right) = C_{Dbasic}\left(\dfrac{S'}{S}\right)\sin^2\alpha \\ C_D = C_{Dbasic}\left(\dfrac{S'}{S}\right)\sin^3\alpha \\ C_L = C_{Dbasic}\left(\dfrac{S'}{S}\right)\sin^2\alpha\cos\alpha \end{cases} \tag{1}$$

where the computation of C_{Dbasic} involves:

1) finding C_{Dbasic} based on Reynolds number;
2) adjusting for compressibility and cross-flow correction to get final C_{Dbasic};
3) correcting the reference area.

TABLE III
AERODYNAMIC STABILITY DERIVATIVES

ALPHA TRIM = 10 deg. (DATCOM)				
Coeff.	M#=0.3	M#=0.6	M#=0.8	M#=2.0
$C_{N\alpha}$	16.094	13.212	10.875	10.015
$C_{N\delta e}$	12.307	12.485	12.124	6.520
$C_{M\alpha}$	-48.106	-46.822	-44.777	-10.279
$C_{M\delta e}$	-123.266	-124.985	-121.278	-67.076
ALPHA TRIM = 40 deg. (DATCOM)				
$C_{N\alpha}$	6.578	44.112	52.443	31.581
$C_{N\delta e}$	5.690	6.452	6.967	4.864
$C_{M\alpha}$	-68.927	-103.362	-104.679	-58.786
$C_{M\delta e}$	-56.992	-64.572	-69.683	-50.008
ALPHA TRIM = 80 deg. (HIGH ALPHA)				
$C_{N\alpha}$	10.796	11.156	11.529	0.0
$C_{N\delta e}$	0.0	0.0	0.0	0.0
$C_{M\alpha}$	0.0	0.0	0.0	0.0
$C_{M\delta e}$	0.0	0.0	0.0	0.0

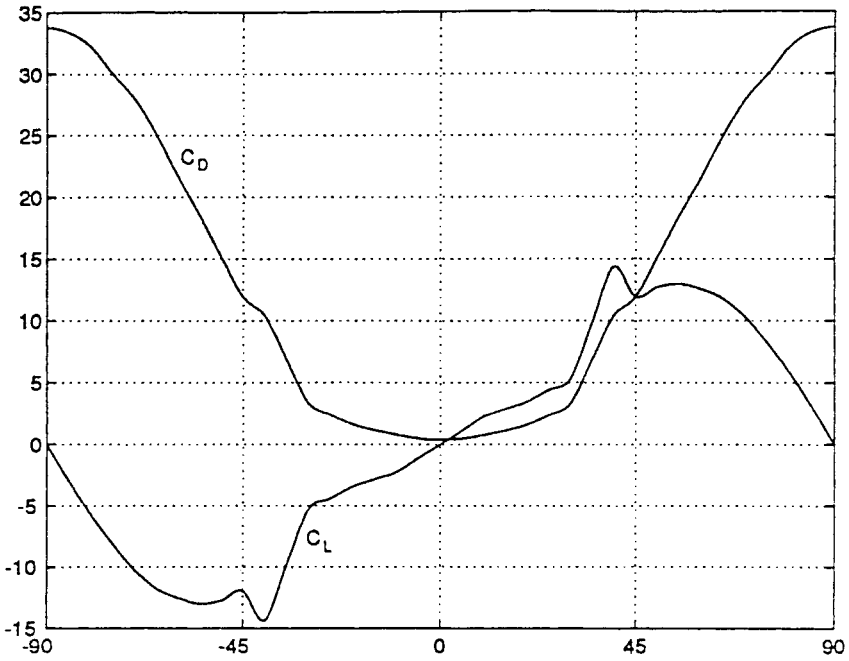

Fig. 3. Aerodynamic forces versus angle of attack.

Table III summarizes the aerodynamic derivatives for various reference values of the angle of attack, and various Mach numbers as computed from [4] and the above prediction techniques. For a reference speed of Mach $= 0.8$, the plots of lift and drag coefficients over a $\pm 90^{\circ}$ range of angle of attack are shown in Fig. 3. The missile is statically stable in the low angle of attack range, at higher angles of attack, where instability may occur, no precise information was available the pitching moment contribution was treated as a disturbance to be compensated by the controller. The rather unconventional maneuver has different possible values for attitude and air flow direction, since the angle of attack can reach values greater than 90°. Its equivalence to the computed interval is given in Fig. 4, and was obtained from geometric considerations.

B. Low Angle of Attack Model

Fig. 5 shows the different coordinate systems used to define the equations of motion. The inertial coordinate system is EXZ and the OX_1Z_1 system translates but is nonrotating. Since OX_1Z_1 is a nonrotating frame, the attitude of the missile can be referenced to that system. The body-fixed rotating system is Oxz. The point O is located at the missile's center of mass. With reference to the assumptions at the beginning of the section, we restrict ourselves to considering the symmetric

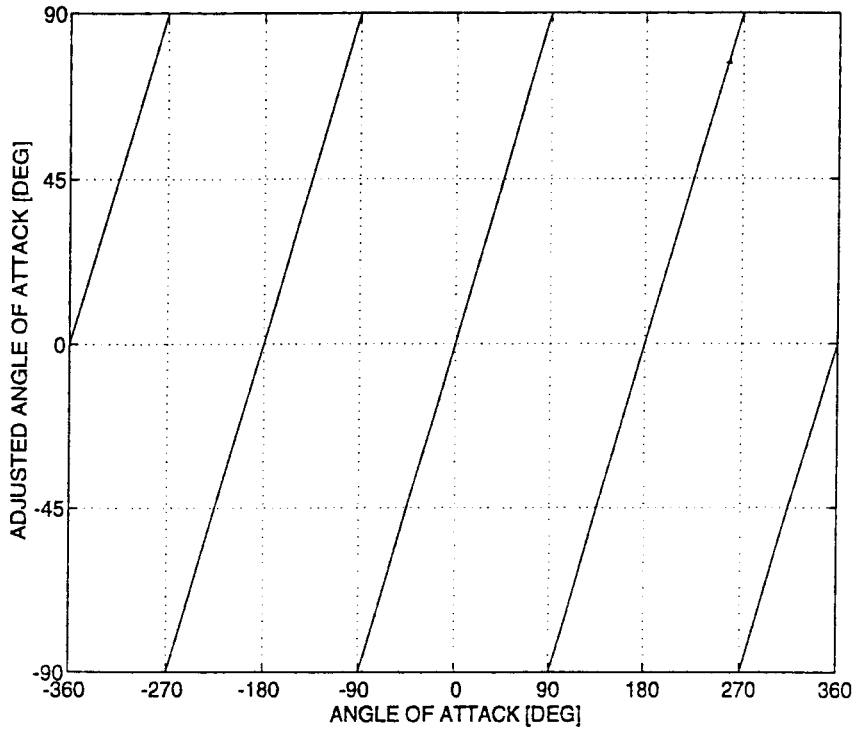

Fig. 4. Angle of attack equivalence.

component of the total motion. The longitudinal equations of motion become therefore

$$\begin{cases} m\ddot{X} = -L\sin\Gamma - D\cos\Gamma + T_E\cos\Theta \\ \qquad - T_{\mathrm{RCS}}\sin\Theta U_T \\ m\ddot{Z} = -L\cos\Gamma + D\sin\Gamma - T_E\sin\Theta \\ \qquad - T_{\mathrm{RCS}}\cos\Theta U_T + mg \\ I_y\dot{Q} = M - (I_x - I_z)PR \\ \dot{\Theta} = Q\cos\Phi - R\sin\Phi \\ \Gamma = \Theta - \alpha \end{cases} \tag{2}$$

where the first two equations describe the translation of its center of mass acted on by lift ($L = \rho V_T^2 S C_L/2$) and drag ($D = \rho V_T^2 S C_D/2$) forces, the main engine thrust (T_E), the reaction jet thrust (T_{RCS}) and gravity, in the *inertial* reference frame. Here, U_T is the throttle variable for the reaction control jets and can have one of the values -1, 0, or 1. The third equation, the moment equation about the point O, describes the attitude of the missile. Here, M is the sum of all the moments acting about the center of mass. The flight path angle, Γ is the angle between the velocity vector and the horizontal X_1 axis. The attitude angle of the missile is Θ, and α is its angle of attack. The last of (2) relates the flight path angle, the pitch angle, and the angle of attack.

From the first two equations, inertial velocities may be obtained by integration, then a second integration provides the inertial coordinates X and Z. The flight path angle can be also determined from the following relationship:

$$\Gamma = -\tan^{-1}\left(\frac{\dot{Z}}{\dot{X}}\right). \tag{3}$$

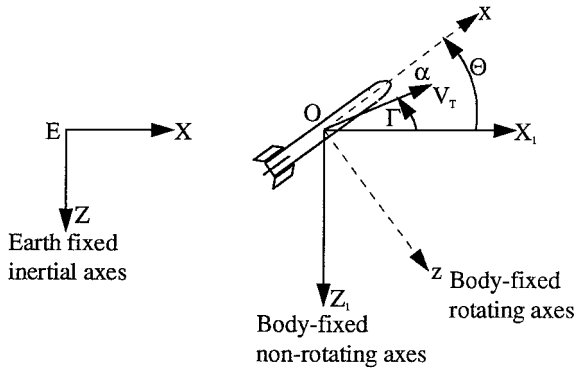

Fig. 5. Reference frames used in the model derivation.

The derivative of (3) with respect to time provides the time rate of change of flight path angle in terms of X, Z, and their time derivatives

$$\dot{\Gamma} = \frac{\dot{Z}\ddot{X} - \ddot{Z}\dot{X}}{\dot{X}^2 + \dot{Z}^2}. \tag{4}$$

The complete nonlinear motion of the missile is thus described by (2)–(4). For the purposes of designing the control system, the translational motion in (2) is rewritten in a more familiar form by using the wind axes reference as

$$\begin{cases} m\dot{V}_m = F_x\cos\alpha\cos\beta + F_y\sin\beta + F_z\sin\alpha\cos\beta \\ \dot{\alpha} = Q + \dfrac{1}{V_m\cos\beta}\left[-PV_m\cos\alpha\sin\beta\right. \\ \qquad \left. - RV_m\sin\alpha\sin\beta - F_x\sin\alpha + F_z\cos\alpha\right] \end{cases} \tag{2'}$$

where $F_i, i = x, y, z$ are the components of the applied forces in body axes and V_m the total velocity of the missile. Assuming no sideslip $\beta = 0$, yields

$$\begin{cases} m\dot{V}_m = F_x \cos\alpha + F_z \sin\alpha \\ \dot{\alpha} = Q + \dfrac{1}{V_m}\left[-F_x \sin\alpha + F_z \cos\alpha\right] \end{cases} \tag{2''}$$

Using the body fixed reference Oxz, (2″) are also written as shown in (5) at the bottom of the page, where u and w are the velocity components along the body axes. Using trigonometric relations and the relation $\alpha = \theta - \Gamma$, the equations may be further simplified leading to

$$\begin{cases} m\dot{u} = -mqw - D\cos\alpha + L\sin\alpha + T_E - mg\sin\Theta \\ m\dot{w} = mqu - D\sin\alpha - L\cos\alpha + T_{\mathrm{RCS}}U_T \\ \qquad\quad + mg\cos\Theta \\ I_y\dot{Q} = M \\ \dot{\Theta} = Q. \end{cases} \tag{6}$$

These are the nonlinear longitudinal equations of motion, they are general except for the fact that roll rate, yaw rate, roll, and sideslip angles do not appear in them because of the assumed motion separation, mentioned above.

From (2″) or (6), classical approximate short-period equations can be derived [7], to be used as baseline for control design by linearizing about the trim condition, with $w \sim V_m\alpha$, and negligible speed perturbation along the x axis small so that the first equation can be dropped. The approximate linear equations then become

$$\begin{cases} \dot{\alpha} = \dfrac{-QS}{mV_T} C_{N\alpha}\alpha + q - \dfrac{QS}{mV_T} C_{N\delta}\delta - \dfrac{T_{\mathrm{RCS}}}{mV_T} u_T \\ \quad = Z_\alpha\alpha + \theta + Z_\delta\delta + Z_T u_T \\ \dot{q} = \dfrac{QSL_{\mathrm{REF}}}{I_y} C_{m\alpha}\alpha + \dfrac{QSL_{\mathrm{REF}}}{I_y} C_{m\delta}\delta + \dfrac{T_{\mathrm{RCS}}L_{\mathrm{RCS}}}{I_y} \\ u_T = M_\alpha\alpha + M_\delta\delta + M_T u_T \\ \dot{\theta} = q \end{cases} \tag{7}$$

with δ the elevator deflection and u_T the RCS input $(+1, -1)$.

T_{RCS} is the thrust provided by reaction jets and L_{RCS} is the jets moment arm. The actuators are modeled by linear first-order systems with time constants τ_d and τ_u for the elevator and RCS, respectively, and given by

$$\begin{cases} \tau_\delta\dot{\delta} = \delta + \delta_c \\ \tau_u\dot{u}_T = u_T + u_{Tc}. \end{cases} \tag{8}$$

Since standard measurements and commands in missile autopilots include accelerometers and rate gyros, (7) and (8) can be rewritten in state-space form by introducing the normal load factor N_z as a state variable replacing the angle of attack. From kinematics, we have

$$N_z = \frac{a_z}{g} = \frac{V_T}{g}(\dot{\alpha} - q). \tag{9}$$

By defining $\overline{x}^T = [N_z \quad q \quad \delta \quad u_T]$ and $\overline{u}^T = [\delta_c \quad u_{Tc}]$ we obtain

$$\begin{bmatrix} \dot{N}_Z \\ \dot{q} \\ \dot{\delta} \\ \dot{u}_T \end{bmatrix} = \begin{bmatrix} Z_\alpha & \dfrac{V_T Z_\alpha}{g} & -\dfrac{V_T Z_\delta}{g\tau_\delta} & -\dfrac{V_T Z_T}{g\tau_u} \\ \dfrac{gM_\alpha}{V_T Z_\alpha} & 0 & M_\delta - \dfrac{M_\alpha Z_\delta}{Z_\alpha} & M_T - \dfrac{M_\alpha Z_T}{Z_\alpha} \\ 0 & 0 & -\dfrac{1}{\tau_\delta} & 0 \\ 0 & 0 & 0 & -\dfrac{1}{\tau_u} \end{bmatrix} \cdot \begin{bmatrix} N_Z \\ q \\ \delta \\ u_T \end{bmatrix} + \begin{bmatrix} \dfrac{V_T Z_\delta}{g\tau_\delta} & \dfrac{V_T Z_T}{g\tau_u} \\ 0 & 0 \\ \dfrac{1}{\tau_\delta} & 0 \\ 0 & \dfrac{1}{\tau_u} \end{bmatrix} \begin{bmatrix} \delta_c \\ u_{Tc} \end{bmatrix}$$

or, in standard form

$$\dot{\overline{x}} = A\overline{x} + B\overline{u} \tag{10}$$

with the output vector being equal to the state vector. The time rate of change of the flight path angle is computed from the normal acceleration, provided α is small, as

$$\dot{\gamma} = -\frac{a_z}{V_T} \tag{11}$$

and the inertial velocity components are

$$\begin{cases} \dot{X} = V_m\cos\gamma \\ \dot{Z} = V_m\sin\gamma. \end{cases} \tag{12}$$

With reference to the above derivation, there are a couple of points that need to be highlighted. First of all, short period approximation has been derived in the hypothesis of small values of angle of attack. Clearly the approximation maintains its validity if α does not become greater than 10–15°. During

$$\begin{cases} m\begin{bmatrix} \dot{u} + qw \\ \dot{w} - qu \end{bmatrix} = \begin{bmatrix} \cos\Theta & -\sin\Theta \\ \sin\Theta & \cos\Theta \end{bmatrix} \begin{bmatrix} -L\sin\Gamma - D\cos\Gamma + T_E\cos\Theta - T_{\mathrm{RCS}}\sin\Theta U_T \\ -L\cos\Gamma + D\sin\Gamma - T_E\sin\Theta - T_{\mathrm{RCS}}\cos\Theta U_T + mg \end{bmatrix} \\ I_y\dot{Q} = M \\ \dot{\Theta} = Q \\ \Gamma = \Theta - \alpha \end{cases} \tag{5}$$

simulation, the complete model given by (2) is used in conjunction with the synthesized autopilot. The short duration of this phase will also mitigate modeling errors. The final simulation will demonstrate the capability of the autopilot in controlling the missile, in the presence of such approximation in the model.

The second point deals with the feedback of actuator signal. In practice this information is not available, however the control design is based on full state feedback and therefore it includes actuator dynamics. This procedure appears realistic at this stage of synthesis, where the major concern is a feasibility study, rather than actual controller implementation.

C. High Angle of Attack Model

For the synthesis of the autopilot during this phase, the starting equations of motion are again given by (2)–(4), with the limitation to longitudinal dynamics. Since an accurate aerodynamic model for this flight regime was not available, a worst-case design was assumed consisting of the predicted normal force at 90° of angle of attack, and the attitude dynamics reduced to that of a double integrator with an external control torque due to the reaction jets and an opposing moment due to the drag. With this in mind, the attitude motion was modeled by

$$I_y \dot{q} = QSC_N L_{cp} + L_{\mathrm{RCS}} T_{\mathrm{RCS}} u_T \tag{13}$$

where L_{cp} is the distance between center of pressure and the center of mass. The value of L_{cp} will be another design parameter for future studies, when a more detailed aerodynamic model will be available. The normal acceleration in this phase is computed during the simulation from inertial information as

$$a_z = \ddot{X} \sin \Theta + \ddot{Z} \cos \Theta. \tag{14}$$

In this phase, the main engine plays a crucial role in the recovery of speed and rotation of the velocity vector. Without this contribution the reaction jet control could not suffice. Whether the main engine is operational at the time of the maneuver, or turned on during the high alpha section of the flight (with the assumption of such a propulsive capability), its contribution does not involve attitude control, and it is therefore considered as an open-loop component as far as the pitch autopilot is concerned.

D. Acquisition of Steady State

At the end of the maneuver, the vehicle enters again the low angle of attack regime with partial recovery of dynamic pressure, and the longitudinal motion is described by (2). For the purpose of autopilot synthesis, however, the short period approximation is modified slightly to account for direct feedback of the flight path angle. This variation is needed if direct control over the speed is required. The model used for control becomes then

$$\begin{cases} \dot{\gamma} = Z_\alpha \gamma - Z_\alpha \theta + Z_\delta \delta + Z_T u_T \\ \dot{q} = -M_\alpha \gamma + M_\alpha \theta + M_\delta M_T u_T \\ \dot{\theta} = q. \end{cases} \tag{15}$$

The autopilot synthesis is based on (15) in order to control steady-state values of attitude, flight path angle, and consequently angle of attack. From a control viewpoint, the flight path angle can be considered an additional input or state, depending on the structure chosen for the autopilot synthesis.

IV. Autopilot Synthesis

This section describes the synthesis of the pitch channel autopilot, the control logic is broken down according to flight phase, resulting in a structure that includes the low alpha component, the post stall rotation, and the final steady-state acquisition. Of course this approach requires synthesizing three controllers, which may not be feasible in actual implementation. The main reason for doing this was the investigation of how well different variable structure control structures would perform, and then leaving the selection of the most appropriate in a future work.

Among the potential theoretical tools for the synthesis, variable structure control (VSC) methods are suggested for several reasons. First of all, the maneuver characteristics present nonlinear dynamics with large parameter variations. Second, the autopilot will require high gain capabilities, due to the maneuver requirements in terms of time of steady-state acquisition. Third, the use of reaction jets, as the main component of the actuation system, leads naturally to the implementation of nonlinear, relay-type logic. VSC, with due care, is one of the methodologies capable of addressing all these issues in a structured framework.

VSC has been described in the former Soviet literature since the early 1960's, see, for example, [8]–[10], among others. Invariance of VSC to a class of disturbances and parameter variations was first developed by Drazenovic in 1969 [11]. In the past two decades, a large amount of research has been performed in the area by the international community [6].

The essential feature of a variable structure controller is that it uses nonlinear feedback control with discontinuities on one or more manifolds (sliding hyperplanes) in the state space, or error space, in the case of model following control. This type of methodology is attractive in the design of controls for nonlinear uncertain dynamic systems with uncertainties and nonlinearities of unknown structure as long as they are bounded and occurring within a subspace of the state space [12]. The basic feature of VSC is the sliding motion. This occurs when the system state continuously crosses a switching manifold because all motion in its vicinity is directed toward the sliding surface. When the motion occurs on all the switching surfaces at once, the system is said to be in the "sliding mode" and then the original system is equivalent to an unforced completely controllable system of lower order.

The design of a variable structure controller consists of several steps: the choice of switching surfaces, the determination of the control law and the switching logic associated with the discontinuity surfaces (usually fixed hyperplanes that pass through the origin of the state space). To ensure that the state reaches the origin along the sliding surfaces, the equivalent system must be asymptotically stable. This requirement defines the selection of the switching hyperplanes (sometimes called

the "existence" problem), which is completely independent of the choice of control laws. The selection of the control law is the so-called "reachability" problem. It requires that the system be capable of reaching the sliding hypersurface from any initial state.

During operation in the sliding mode, the discontinuous control chatters about the switching surface at high frequency. Chatter is the major problem associated with this type of control. Execution of control commands may require high energy effort from the actuators, thus leading to continuous saturation. It can also excite neglected high-order dynamics. This is perhaps the reason why VSC has not yet found wider acceptance in the flight control community, where smoothness of actuation is desirable to avoid saturation and, possibly, instability. The introduction of discontinuous actuators such as reaction jets and active flow control is, however, changing this perspective and variable structure systems are being viewed as a viable alternative to traditional relay control strategies.

There are several ways to mitigate the effects of chattering, with little loss in performance. These include the definition of a boundary layer near the sliding surface as introduced in [13], and/or the introduction of a smoothing parameter in a unit vector-type control law as shown in [12] and [14]–[16]. The latter approach is used in the present work. As noted in [17], the smoothing factors do not guarantee full robustness, however such relaxation is the price paid for avoiding actuator saturation. Of course, smoothing is not necessary when on–off actuators such as thrusters are being used.

The flight condition chosen for point design corresponds to Mach 0.8 and altitude of 10 000 ft. The design goal is a controller structure, insensitive to the uncertainty on the values of the aerodynamic coefficients in order to limit gain scheduling. As mentioned earlier, since the main aim of the work was to test variable structure control logic, three different structures are considered. In the initial phase a g-command autopilot is synthesized, during the high alpha rotational portion an attitude following autopilot is used, and finally, in the low alpha final phase a model following with flight path information is synthesized. In addition, the three phases differ in their implementation, while the first and third use both reaction jets and elevator; the second-phase control relies on the use of reaction jets. In all cases, the main engine is used when the speed falls below a preassigned value, since it is assumed that initial and final velocity be the same.

A. Phase I Autopilot

Using the numerical values corresponding to the nominal flight condition, the system's matrices in (10) become

$$A = \begin{bmatrix} -0.1647 & -4.4082 & 884.6 & 1109.1 \\ 7.5829 & 0 & -53.27 & 47.87 \\ 0 & 0 & -180 & 0 \\ 0 & 0 & 0 & -500 \end{bmatrix}$$

$$B = \begin{bmatrix} -884.6 & -1109.1 \\ 0 & 0 \\ 180 & 0 \\ 0 & 500 \end{bmatrix}.$$

The autopilot objective in this phase is the tracking of a g-command to achieve a rapid change in acceleration. In this respect, the autopilot does not differ from other traditional missile autopilots [7]. The main reason for choosing a g-command structure strategy was to preserve the control logic available from standard designs and used in parts of the flight envelope not requiring post stall maneuvering, nor reaction jets. Although not strictly necessary for this particular maneuver, an integrator is added to the state vector in order to ensure perfect tracking of the load factor, leading to a VSC-PI type control structure with state vector $\overline{x}_{\text{aug}}^T = [\int N_z dt \quad N_z \quad q \quad \delta \quad u_T]$. The augmented system dynamics are

$$\dot{\overline{x}}_{\text{aug}} = A_{\text{aug}}\overline{x}_{\text{aug}} + B_{\text{aug}}\overline{u}. \tag{16}$$

The VSC structure chosen for the controller has the form [12], [16]

$$\overline{u} = -L\overline{x}_{\text{aug}} - \rho \frac{N\overline{x}_{\text{aug}}}{||M\overline{x}_{\text{aug}}|| + \varepsilon} \tag{17}$$

where the gain matrices are computed using optimal control, and the design parameters ε and ρ are selected based on response speed considerations (for their numerical values see [1]). Since the reaction jets operate in an on–off fashion, their actuation is implemented not according to (18) but as function of the sign of the sliding surface $\overline{s} = G\overline{x}_{\text{aug}}$ obtained by the VSC design. The stability of the system is ensured provided the reaction jet equivalent control remains bounded between $+1$ and -1 [18]. A block diagram of the autopilot structure for this phase is shown in Fig. 6.

B. Phase II Autopilot

This phase is characterized mainly by a pure rotation in pitch generated by RCS alone. In this phase, the vehicle is operating at angles of attack above stall and the aerodynamic forces and moments are assumed to have negligible effect in the control of the missile. The main objective of the autopilot in this phase is the rotation of the vehicle and compensation of dynamic pressure, which drops considerably due to speed reduction associated with drag increase at high angles of attack. To recover dynamic pressure, the main engine is fired in an open-loop fashion. If a single boost engine is present, the engine is on during the entire maneuver, if multiple-boost capability is available, then the engine is fired at a predetermined attitude (in our case chosen nominally equal to 120°). The engine remains in a boost phase mode until the final desired speed (here assumed equal to the initial one) is achieved as well as the appropriate direction of flight. The equations of motion used for the controller synthesis are (6) and (13). VSC is applied to (13), which can be written in state-space form as

$$\begin{aligned} \dot{\overline{x}} &= \begin{bmatrix} \dot{\theta} \\ \dot{q} \end{bmatrix} \\ &= \begin{bmatrix} 0 & 1 \\ 0 & 0 \end{bmatrix} x + \begin{bmatrix} 0 \\ \dfrac{L_{\text{RCS}} T_{\text{RCS}}}{I_y} \end{bmatrix} u_T + \begin{bmatrix} 0 \\ \dfrac{QSC_N L_{\text{CP}}}{I_y} \end{bmatrix} \\ &= A\overline{x} + Bu_T + D. \end{aligned} \tag{18}$$

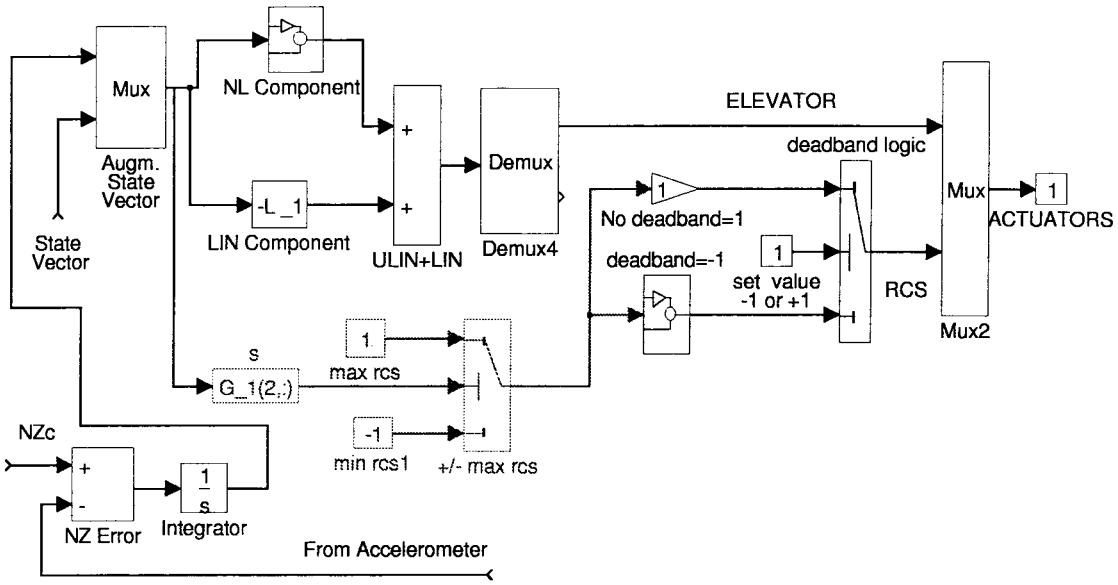

Fig. 6. Autopilot block diagram for Phase I.

Globally, the torque due to normal force produces a resisting effect that can be treated as a disturbance D. To perform a point design of the autopilot, a worst case approach was used and D was bounded by the value corresponding to a cylinder set perpendicular to the flow, where the drag assumes its maximum value. With this, the B and D terms in (18) become

$$B = \begin{bmatrix} 0 \\ 31.049 \end{bmatrix}, \; D = \begin{bmatrix} 0 \\ -10 \end{bmatrix}.$$

Next, VSC is applied using a model following approach [12], [19], by specifying a desired model for the pitch rotational dynamics chosen as

$$\begin{aligned} \dot{\overline{x}}_m &= A_m \overline{x}_m + B_m u_m \\ &= \begin{bmatrix} 0 & 1 \\ -178 & -24 \end{bmatrix} \overline{x}_m + \begin{bmatrix} 0 \\ 178 \end{bmatrix} u_m \end{aligned} \tag{19}$$

from (17) and (18), the error dynamics $\overline{e} = \overline{x}_m - \overline{x}$ are given by

$$\dot{\overline{e}} = A_m \overline{e} + [A_m - A]\overline{x} + B_m u_m - D - B u_T. \tag{20}$$

In the present case, unlike [19], the implementation of the control law in (19) is given simply by the nonlinear component, since reaction jets take only -1, 0, $+1$ values. Dropping the linear term yields

$$\begin{cases} u_T = u^{NL} = \operatorname{sgn}(s) \\ s = G\overline{e} = [7 \; 1]\overline{e}. \end{cases} \tag{21}$$

The choice of G was made so as to ensure a desirable response during sliding. Phase II starts with initial conditions corresponding to the state variables final conditions from Phase I. At the end of Phase II, the angle of attack is below stall and Phase III autopilot becomes active.

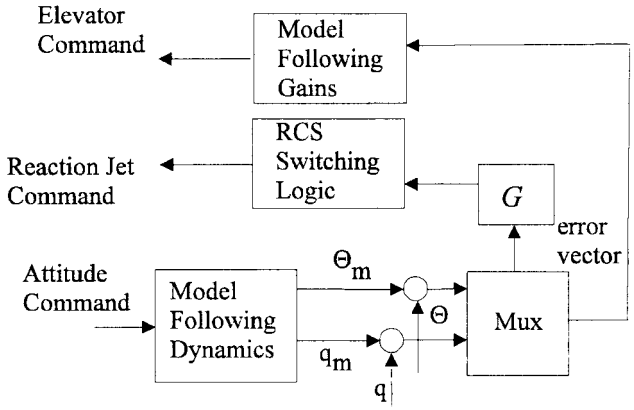

Fig. 7. Autopilot block diagram beyond stall.

C. Phase III Autopilot

This phase involves the task of acquiring and maintaining a set of steady-state values for the attitude and flight path of the vehicle. In our work we established the objective of reaching 180 of flight path and attitude angles, although different values can be set as desired. The vehicle dynamics are modeled by the linearized system given by (7). The flight path angle, necessary since the velocity of the vehicle can not be considered to be constant, is introduced in the equations of motion as a disturbance term. Using a model following approach to the autopilot synthesis, we have

$$\begin{aligned} \begin{bmatrix} \dot{\Theta} \\ \dot{q} \end{bmatrix} &= \begin{bmatrix} 0 & 1 \\ -33.4266 & 0 \end{bmatrix} \begin{bmatrix} \Theta - \theta_0 \\ q \end{bmatrix} + \begin{bmatrix} 0 & 0 \\ -90.536 & 31.049 \end{bmatrix} \\ &\quad \cdot \begin{bmatrix} \delta \\ u_T \end{bmatrix} + \begin{bmatrix} 0 \\ -33.4266 \end{bmatrix} \gamma \\ \begin{bmatrix} \dot{\theta}_m \\ \dot{q}_m \end{bmatrix} &= \begin{bmatrix} 0 & 1 \\ -36.4 & -12 \end{bmatrix} \begin{bmatrix} \theta_m \\ q_m \end{bmatrix} + \begin{bmatrix} 0 \\ 36.4 \end{bmatrix} u_m \end{aligned} \tag{22}$$

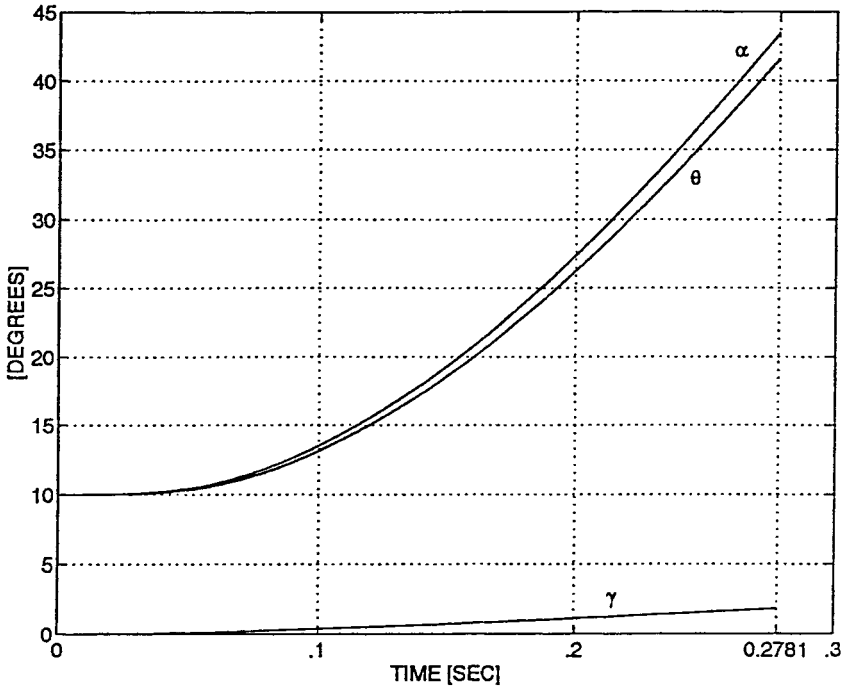

Fig. 8. Angular motion below stall.

the control procedure is similar to the previous one leading to a structure of the form

$$\begin{cases} \delta = K_x(X - x_0) + K\gamma(\Gamma - \gamma_0) + K_{um}(U_m - u_{m0}) \\ u_T = \begin{cases} 1, (s > 0) \\ 0, (s = 0) \\ -1, (s < 0) \end{cases} \end{cases} \tag{23}$$

with $s = G\underline{e} = 7(\theta_m - \theta) + (q_m - q)$. Note that the elevator is responsible for providing model following, while the reaction jet control gives robustness to parameter variations and disturbances. The choices of model dynamics and sliding surface depend on the desired response and they can be considered as design parameters. The autopilot schematic for this phase is shown in Fig. 7.

V. Simulation Results

The autopilot synthesis, described in the previous section, was tested with a nonlinear simulation code developed in the Matlab®-Simulink environment. The main objectives of the simulation were to validate the autopilot performance in the chosen scenario, to test the robustness of the methodology by using fixed controller gains instead of gains scheduled with angle of attack and Mach number, and to verify the robustness of the methodology with respect to parameter variations such as reference speed, initial time of main engine firing, and reaction jet reference thrust.

It is important to note that, during the simulation, the aerodynamic forces and moments are not constant, but vary according to Fig. 3, as functions of the angle of attack.

The maneuver begins with a negative 5 g N_{zc} command. The missile pitches up reaching stall within 0.278 s from the beginning of the maneuver. The motion is mainly in pitch with no appreciable change in flight path angle as seen from Fig. 8 where pitch, flight path, and angle of attack are plotted. The load factor at stall has almost reached the commanded value of five times the gravity acceleration resulting in a controller, where the sliding surface has not been reached yet.

Once in the stalled phase (preselected to be 40° of angle of attack), the autopilot becomes a second-order model following VSS. The missile responses in attitude, angle of attack, and flight path angle are given in Fig. 9. In this phase, the main engine is activated when the attitude angle reaches a value of 120°, just prior to 0.5 s. The effect of the engine is clearly evident in the figure. The Phase II trajectory is shown in Fig. 10. The solid line shows the trajectory followed by the center of mass. The missile icon shows the attitude at various points. The velocity vector is shown by the vector lines, with the length of the vector being indicative of its magnitude.

The final phase is the acquisition of steady-state conditions. The key variables here are the pitch angle and the flight-path angle, which are required to reach a value of 180°. The resulting complete trajectory is shown in Fig. 11, while Fig. 12 contains time histories of the angular displacements, speed, and control effort throughout the maneuver.

In order to visualize some of the payoffs of a post stall maneuver, compared to conventional ones, the heading reversal is compared with a traditional turn obtained using a typical

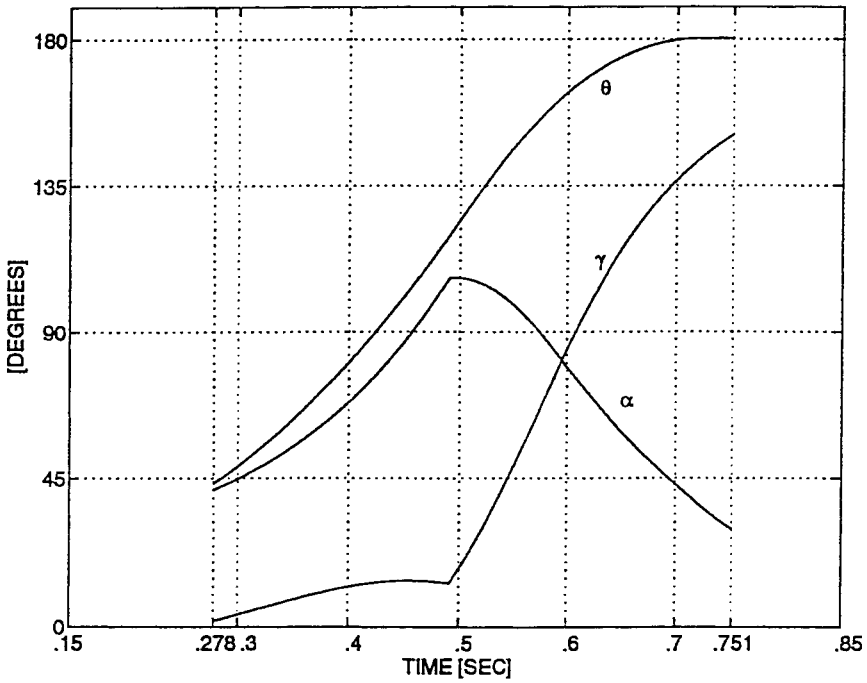

Fig. 9. Angular motion during Phase II.

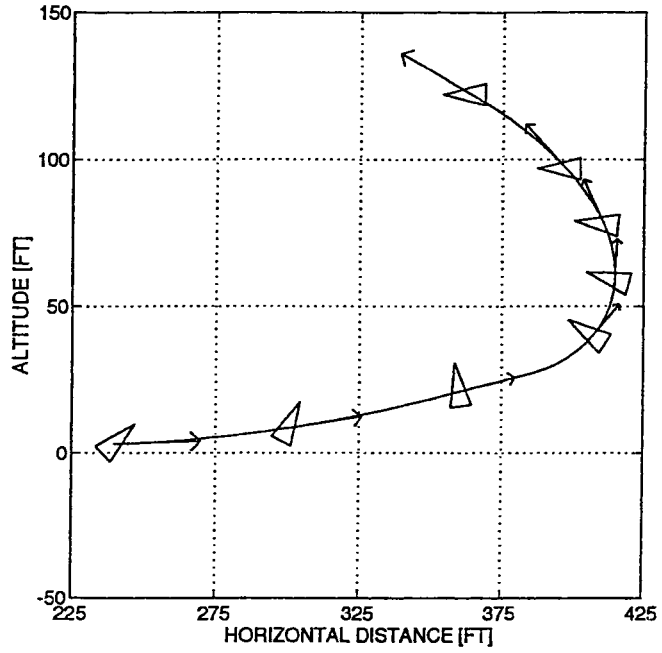

Fig. 10. Trajectory during Phase II.

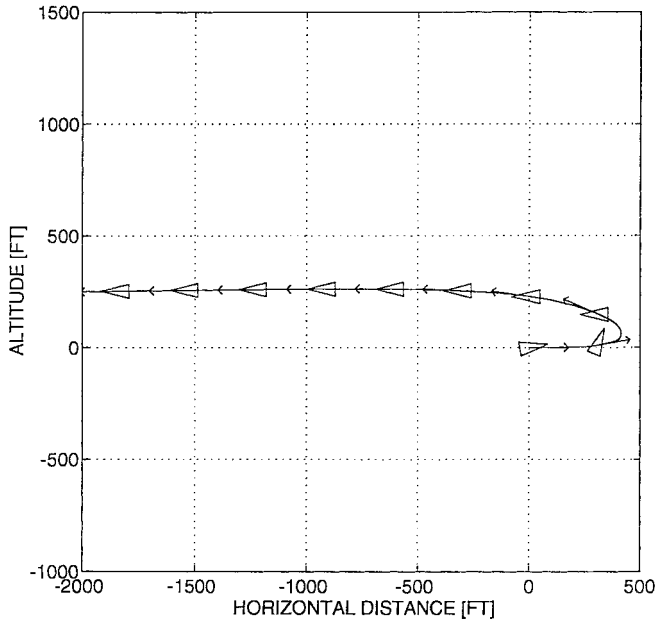

Fig. 11. Complete trajectory.

g-command autopilot. Although qualitative, in the sense that the g-command maneuver was not optimized, the advantage of using RCS in conjunction with fins is evident, as shown by Fig. 13. The turn radius is of the order of 15 000 feet and the time necessary for the maneuver is about 50 s. The main reason for the insufficiency of a standard g-command autopilot lies in the fact that the reduced fin size does not allow a generation of load factors large enough for a more efficient trajectory. Details on the g-command autopilot can be found in [20].

VI. Conclusions

A pitch channel missile autopilot has been synthesized, which uses a combination of aerodynamics and propulsive controls (in the form of reaction jet thrusters), in order to perform a high angle of attack maneuver consisting of a

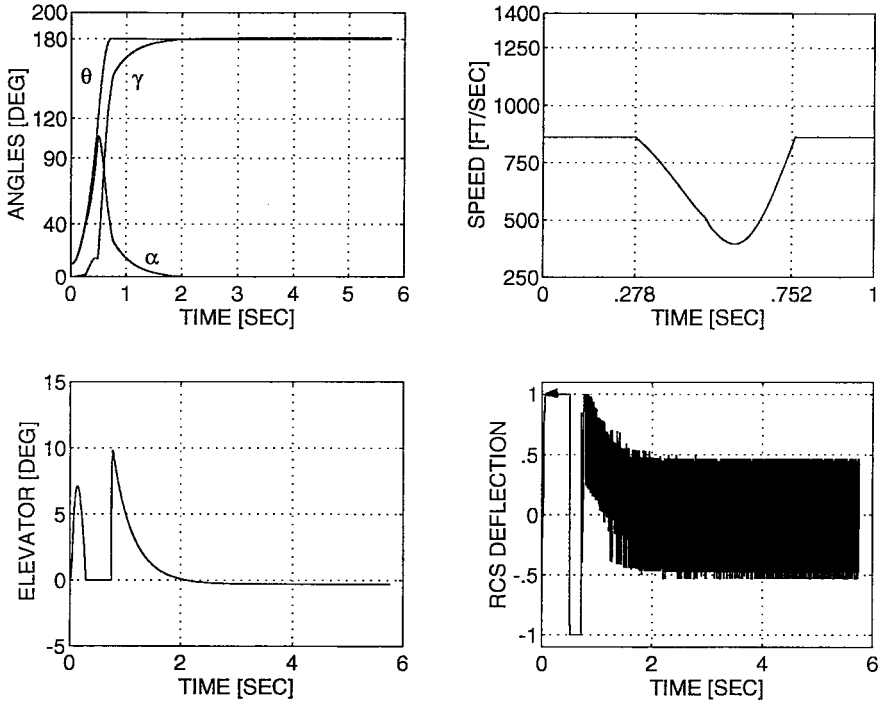

Fig. 12. Time histories for the entire trajectory.

180° heading reversal. The autopilot uses variable structure control methods, and changes logic according to the missile being below or above the stall region. This approach to the synthesis was chosen primarily in order to evaluate the performance of variable structure methods using different frameworks (proportional-integral tracking, and model following). Dynamic pressure loss is recovered by the main engine according to the attitude of the missile, or by performing the maneuver during boost phase. Autopilot performance are validated via nonlinear simulation, showing the robustness with respect to aerodynamic uncertainties and speed variations. Current work [20] indicates that the autopilot gains do not require scheduling even in the presence of varying flight conditions (initial reference speed), reaction jet thrust, and main engine main thrust values. Future work is directed toward the extension of the design to the three-dimensional case, to the selection of the best VSC structure, and to the problem of output feedback, since the autopilot presented in this work assumes full state availability.

APPENDIX

This Appendix contains the autopilot gain matrices used in the paper.

A. Phase I Autopilot

The gain matrices used in (15) are

$$L_1 = \begin{matrix} -5.3517\text{e}-03 & -1.1120\text{e}-02 & -1.2727\text{e}-03 \\ -9.5270\text{e}-01 & -3.6759\text{e}-02 & \\ -4.9005\text{e}-03 & -2.6377\text{e}-03 & -2.6132\text{e}-03 \\ -2.1420\text{e}-02 & -9.8215\text{e}-01 & \end{matrix}$$

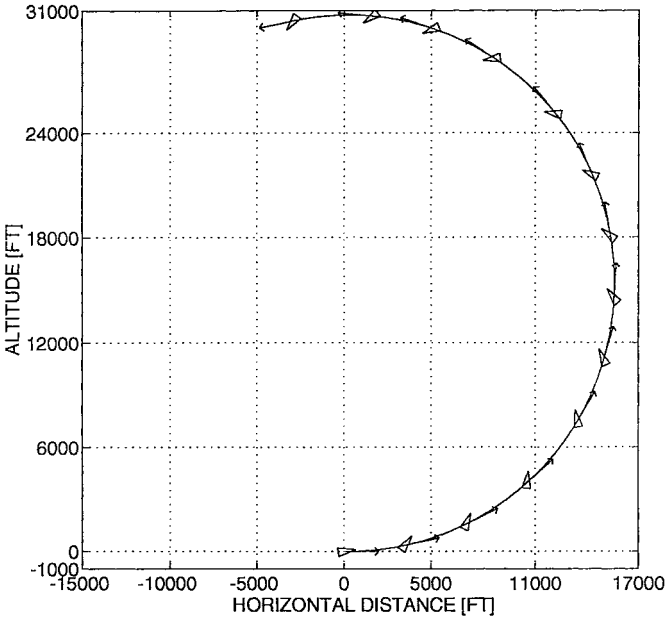

Fig. 13. Comparison with conventional G-command maneuver.

$$M_1 = \begin{matrix} -1.3396\text{e}+00 & -1.4005\text{e}-01 & 9.7002\text{e}-02 \\ -6.8826\text{e}-01 & 2.3606\text{e}-01 & \\ 5.0787\text{e}+00 & 2.2726\text{e}-01 & 1.5613\text{e}-01 \\ -1.3907\text{e}+00 & -5.8274\text{e}-01 & \end{matrix}$$

$$N_1 = \begin{matrix} -2.6758\text{e}-03 & 5.6661\text{e}-05 & -3.8657\text{e}-04 \\ 3.0562\text{e}-03 & 1.2569\text{e}-04 & \\ -2.4502\text{e}-03 & -2.5616\text{e}-04 & 1.7742\text{e}-04 \\ -1.2589\text{e}-03 & 4.3177\text{e}-04. & \end{matrix}$$

The gain matrix G defining the sliding surface is given by

$$G_1 = \begin{matrix} -2.6792\text{e}+00 & -2.8010\text{e}-01 & 1.9400\text{e}-01 \\ -1.3765\text{e}+00 & 4.7212\text{e}-01 & \\ 1.0157\text{e}+01 & 4.5452\text{e}-01 & 3.1226\text{e}-01 \\ -2.7815\text{e}+00 & -1.1655\text{e}+00. & \end{matrix}$$

B. Phase III Autopilot

The model to be followed has a second-order dynamics. The gains in (21) are given by: $K_{x-3} = [3.2843\text{e}-02 \quad 1.3254\text{e}-01]$, $K_{um-3} = -4.0205\text{e}-01$, $K_{\gamma-3} = -3.6921\text{e}-01$.

The gain G defining the sliding surface is in this case: $G_3 = [7 \quad 1]$.

ACKNOWLEDGMENT

M. Innocenti wishes to thank F. A. Davis, branch chief, WL/MNAV, Eglin AFB, FL, for the helpful comments, and two anonymous reviewers for their detailed revisions and suggestions.

REFERENCES

[1] M. Innocenti and A. Thukral, "Simultaneous reaction jet and aerodynamic control of missile systems," in *AIAA-93-3739 Guidance, Navigation, and Contr. Conf.*, Monterey, CA, Aug. 1993.
[2] M. Innocenti, "Preliminary missile autopilot using reaction jet and aerodynamic control," AFOSR Summer Faculty Program, Wright Lab., Armament Directorate, Eglin AFB, Final Rep. RDL-33, Aug. 1992.
[3] M. Polites, D. Groll, and J. Evers, "Recent events in guidance, navigation, and control," in *AIAA Guidance, Navigation, and Contr. Conf.*, San Diego, CA, July 1996.
[4] K. D. Bruns *et al.*, "Missile DATCOM," Wright Lab., Tech. Rep. WL-TR-91-3039.
[5] S. Hoerner, *Practical Information on Fluid Dynamic Drag.* New York: Wiley, 1958.
[6] A. Thukral, "Design of missile autopilot flight control systems using variable structure techniques," Ph.D. dissertation, Dept. Aerospace Eng., Auburn University, AL, May 1995.
[7] J. H. Blakelock, *Automatic Control of Aircraft and Missiles.* New York: Wiley, 1991.
[8] S. V. Emel'yanov, "Design of variable structure control systems with discontinuous switching functions," *Eng. Cybern.*, vol. 1, 1964.
[9] V. I. Utkin, *Sliding Modes and Their Application in Variable Structure Systems.* Moscow: MIR, 1978.
[10] U. Itkis, *Control Systems of Variable Structure.* New York: Wiley, 1976.
[11] B. Drazenovic, "The invariance condition in variable structure systems," *Automatica*, vol. 5, pp. 287–295, 1969.
[12] A. S. I. Zinober, "Deterministic control of uncertain systems," in *Inst. Elect. Eng.-40, Contr. Eng. Series.* London, U.K.: Peter Peregrinus, 1990.
[13] J. J. E. Slotine and W. Li, *Applied Nonlinear Control.* Englewood Cliffs, NJ: Prentice-Hall, 1990.
[14] G. Ambrosino, G. Celentano, and E. Garofalo, "Variable structure model reference adaptive control systems," *Int. J. Contr.*, vol. 39, no. 6, 1984.
[15] A. Balestrino, G. De Maria, and A. S. I. Zinober, "Nonlinear adaptive model following control," *Automatica*, vol. 20, no. 5, 1984.
[16] A. Thukral and M. Innocenti, "Controls design challenge: A variable structure approach," *AIAA J. Guidance, Contr., Dynamics*, vol. 31, no. 5, Sept./Oct. 1994.
[17] J. Y. Hung, W. Gao, and J. C. Hung, "Variable structure control: A survey," *IEEE Trans. Ind. Electron.*, vol. 40, Feb. 1993.
[18] H. Buhler, "Sliding mode control with switching command devices," *Deterministic Control of Uncertain Systems, IEE-40*, Control Engineering Series. London, U.K.: Peter Peregrinus, 1990.
[19] S. K. Mudge and R. J. Patton, "Enhanced assessment of robustness for an aircraft's sliding mode controller," *AIAA J. Guidance, Contr., Dynamics*, vol. 11, 1988.
[20] M. Innocenti and A. Thukral, "Variable structure autopilot for high angle of attack maneuvers, using on–off thrusters," in *33rd Contr. Decision Conf.*, Lake Buena Vista, FL, Dec. 1994.

Ajay Thukral received the B.S> degree from the Indian Institute of Technology, Kharagpur, in 1986. He received the Master's degree in aerospace engineering in 1991 and the Ph.D. degree in 1995 from Auburn University, AL.

He was an Assistant Professor at Tuskegee University, AL, from 1995 to 1997. He is currently a Programmer Analyst for Boeringer Mannheim, Indianapolis, IN. His research interests include aerospace and biotechnology systems modeling and control.

Mario Innocenti (M'79) received the Laurea degree in aeronautical engineering from the University of Pisa, Italy, in 1977 and the Ph.D. degree in Aeronautics and Astronautics from Purdue University, West Lafayette, IN, in 1982.

He worked for Aeritalia Space Division, Turin, Italy, in 1977. From 1982 to 1984 and 1987 to 1992, he was on the Faculty of Auburn University, AL, Department of Aerospace Engineering, first as an Assistant Professor and later as a tenured Associate Professor. From 1984 to 1987, he held a research position in the Aerospace Engineering Department at the University of Pisa. Since 1993, he has been an Associate Professor in the Electrical Systems and Automation Department of the University of Pisa, where he chairs the course of process control. He has coauthored more than 60 technical papers and manages research activities in control theory, robotics, aerospace, and vehicle control, process control, and optimization. His current interests include nonlinear dynamics and control, robustness, neural networks, and real-time control.

Dr. Innocenti is an Associate Fellow of AIAA, an international member of the *Journal of Guidance, Control, and Dynamics*, and member of the AIAA guidance, navigation, and control technical committee. He has served in several AGARD working groups and lecture series, and he is currently a member of the flight vehicle integration panel.